Analysis of Topographic Amplification Effects on Canyon Sites Using 3D Boundary Element Method

Reza Tarinejad, Mohammad T. Ahmadi, and Naser Khaji

Civil Engineering Department, Tarbiat Modares University, Tehran, I.R. Iran,
email: tari_r@modares.ac.ir

ABSTRACT: *Topographic conditions play an important role on the modification of seismic ground motion. Therefore, their effects may become crucial in the selection or simulation of ground motion for use in structural seismic response analysis. In this research, topography effects of canyon sites are analyzed using a three-dimensional boundary element procedure. The multi-domain boundary element method proposed by Ahmad and Banerjee is used for three-dimensional cases with good accuracy. Effects of model parameters (free-field and canyon lengths) are well accounted for ensuring accurate results. It is shown that the free-field (both side of the canyon cross-section) length is less influential than the canyon length. Some general rules for the three-dimensional boundary element modeling of wave scattering problem are proposed. In addition, effects of different wave parameters (frequency and direction), material properties (damping ratio and poisson's ratio) and canyon geometry are investigated.It is demonstrated that the effect of canyon shape and canyon depth on the topographic amplification is frequency dependent. Deep canyon (semi-circular canyon) induces larger amplification effect than shallow canyon (semi-elliptical canyon) in different frequencies.*

Keywords: Scattering; Seismic Wave; Boundary Element Method; Topographic Amplification; Prismatic Canyon; 3D-model

1. Introduction

Topographic amplification plays an important role on the modification of seismic ground motion. This effect may become crucial in the selection or simulation of ground motion for use in structural seismic response analysis. The effects of surface topography can greatly enlarge the site response exerting an important influence on the distribution of damage observed during earthquakes [1]. Some seismic codes are concerned about the importance of topographic effects [2]. In the last decades the evaluation of topographic effects was done via different approaches. Different analytical and numerical techniques were adopted to deal with topographic effects on the seismic wave scattering problems (e.g., Trifunac [3], Pedersen et al [4], Sanchez-Sesma and Luzon [5], Sanchez-Sesma and Campillo [6], Paolocci [7], Zhang and Chopra [8],

Niu and Dravinski [9] Dravinski [10] Eshraghi and Dravinski [11] Mossessian and Dravinski [12], Zhao et al [13], Luco et al [14], Athanasopoulos et al [15], Assimaki, et al [16], Kamalian et al [17-18], and Geli et al [19]). On the other hand, the recorded ground motions after recent destructive earthquakes have made empirical estimation of topographical effect possible (e.g., March 3rd, 1985 Chile Earthquake [1], June 15th, 1995 Egion Earth-quake in Greece [15], the 1999 Athens Earthquake in Greece [16], the 1994 Northridge Earthquake in California [20], the Dead sea rift earthquake in Israel [21], June 11th, 1999 Earthquake in France [22] and November 23rd, 1980 Earthquake in Italy [23-24]).

Comparisons between theoretical and empirical results for different site responses have been investigated by several studies (e.g., [7, 16 and 19]).

There are some discrepancies on the results obtained from both approaches. Pedersen et al [25] concluded that there is a good agreement between empirical data and theoretical results, concerning purely topographical induced amplifications on ridge tops. On the contrary, Chavez-Garcia et al [26] pointed out a possibility of discrepancy between the horizontal to vertical spectral ratio (*HVSR*) empirical response and the theoretical transfer function, due to the fact that the 2D homogeneous model used in the work may be too simplistic for the mountain under investigation. This latter discrepancy is discussed again in [27] in terms of the inadequacy of the 2*D* models.

A quantitative result obtained for differences between theoretical and observed amplifications at topographic features is presented by Paolocci et al [28]. The limitations of the theoretical simulations on complex sites and lack of enough information of underground irregularities are presented as reasons for disparity [7, 19]. An up-to-date review paper of the published literatures on boundary integral equations and boundary element methods in elastodynamics is recently presented by Bouchon and Sanchez-Sesma [29].

The analytical methods are restricted to media with simple geometries as well as scalar wave components. On the other hand numerical techniques can be used for real-world geometries and vector wave components but they need much computational time and memory. For infinite problems, we need to model a large part of the media with huge degrees of freedom especially using the domain methods such as the finite element. However, the boundary element method (*BEM*) is very effective when dealing with wave propagation problems in infinite media with geometrical irregularities. The main advantage of this method is that discretization is only applied at the boundaries of the physical domain, thus reducing

the number of unknown variables significantly in comparison to other methods such as finite element and finite difference techniques. On the other hand, since the fundamental solutions automatically satisfy the far-field conditions, the *BEM* is especially well-suited to problems involving infinite domains such as a canyon located on a half-space [32]. Issues such as the reduction of dimensionality, the fulfillment of radiation conditions at infinity, and higher accuracy in the results, make the boundary element method quite attractive in engineering seismology and especially in evaluation of topographic effects.

While numerous studies have been done on the two-dimensional elastic response of an isotropic medium, very little has been published on three-dimensional analyses. In this research the multi-domain boundary element method proposed in [30] is used to study the amplification of elastic waves by a three dimensional canyon. Incident plane harmonic *SH*-waves are considered. The accuracy of the method is verified against results of other studies, and effects of different parameters are investigated.

2. Topography

An arbitrarily shaped canyon of finite length located in homogenous, elastic and isotropic half space is considered as illustrated in Figure (1). Seismic body waves arrive from an arbitrary direction with angles of θ_h and θ_v with respect to the horizontal *x*- and the vertical *z*-axes, respectively. The half-space is characterized by the *P* and *S* wave velocities c_p and c_s, respectively. To compute the total displacement at the canyon site due to incident body waves, the following four steps should be taken:

1. Determine the ground motion for free-field conditions (u_{ff}) for the half-space without the canyon, see Figure (2a). Closed-form solutions are available for various incident body waves.
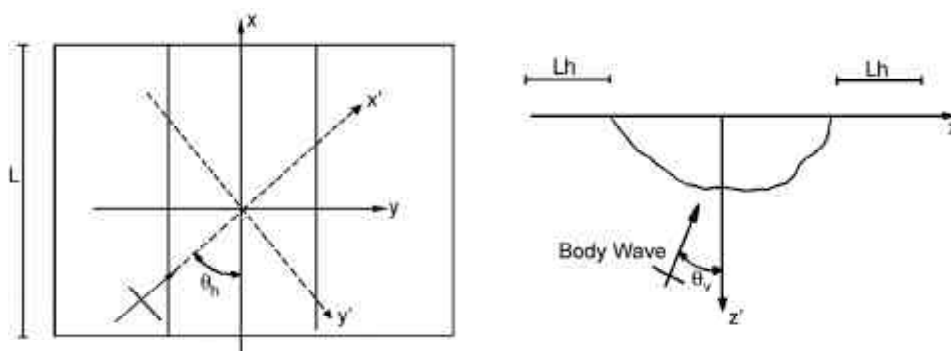

Figure 1. Topographic system considered is an arbitrarily shaped canyon of finite length with the incident waves arriving from an arbitrary direction.

2. Determine the canyon base tractions corresponding to the displacements in the previous step, see Figure (2b).
3. Apply the opposite of the tractions computed in step 2 at the base of the canyon as a traction boundary condition and determine the displacements, see Figure (2c).
4. Determine the total displacements by superposition of the two displacements obtained in steps 1 and 3, i.e., $u_{total} = u_{ff} + u_s$.

In the third step, u_s is determined using the 3D boundary element technique as discussed in the next sections.

3. Background Theory and Boundary Element Method

The governing wave equation in frequency domain for elastic, isotropic and homogeneous body is:

$$c_1^2 \nabla(\nabla \overline{u}) - c_2^2 \nabla \times \nabla \times \overline{u} + \omega^2 \overline{u} = -b \qquad (1)$$

in which $\overline{u}$ denotes the displacement amplitude vector, b denotes the body force vector, ω denotes

Figure 2. Superposition principle for wave scattering problem in a canyon: a) free-field without canyon; b) tractions induced by free-field displacements; and c) displacements due to reversed free-field tractions on the canyon surface.

the circular frequency and c_1 and c_2 are the propagation velocities of compression (P) and shear (S) waves, respectively. The velocities are related to the properties of the medium through:

$$c_1 = (\lambda + 2\mu/\rho)^{0.5}, c_2 = (\mu/\rho)^{0.5} \qquad (2)$$

where λ and μ are the Lame constants and ρ is the mass density [31-32].

The corresponding governing boundary equation for an elastic, isotropic, homogenous body can be obtained using the well-known dynamic reciprocal theorem as:

$$c^i u^i + \int_G p^* u d\mathbf{G} = \int_G u^* p d\mathbf{G} \qquad (3)$$

where c^i is the jump tensor and dependent on the local geometry, p^* and u^* are the fundamental solution for traction and displacement respectively, at a point x when a unit Dirac Delta load is applied at point *i*. In the *BEM*, the variables u and p are discretized into the values at the so-called *collocation nodes*.

The displacement and traction fields are interpolated over each element using a set of shape functions. The same shape functions are also used to approximate the geometry, i.e. the elements are isoparametric. Dicretization of Eq. (3) yields:

$$c^i u^i + \sum_{j=1}^{ne} \left\{ \int_{G_j} p^* \mathbf{F} d\mathbf{G} \right\} u^j = \sum_{j=1}^{ne} \left\{ \int_{G_j} u^* \mathbf{F} d\mathbf{G} \right\} p^j \qquad (4a)$$

The expressions inside the braces can be replaced with the more familiar abbreviations:

$$G^{ij} = \int_{G_j} u^* \mathbf{F} d\mathbf{G} \qquad (4b)$$

$$\hat{H}^{ij} = \sum_t \int_{G_j} p^* \mathbf{F}_k d\mathbf{G} \qquad (4c)$$

$$\begin{cases} H^{im} = \hat{H}^{im} & when \quad i \neq m \\ H^{im} = \hat{H}^{im} + c^i & when \quad i = m \end{cases} \qquad (4d)$$

According to Eq. (4) the surface integral is exchanged with a sum of integrals over *ne* elements. It should be noted that the *BEM* allows the use of *constant* elements, where the displacements and tractions are assumed to be constant over the entire element leading to discontinuities at the element edges. However, this kind of element is inadequate for most wave propagation problems as the convergence is very slow compared to that of higher-order elements. *Quadratic* elements are used in this research. After assembling all equations, the following set of equations is obtained:
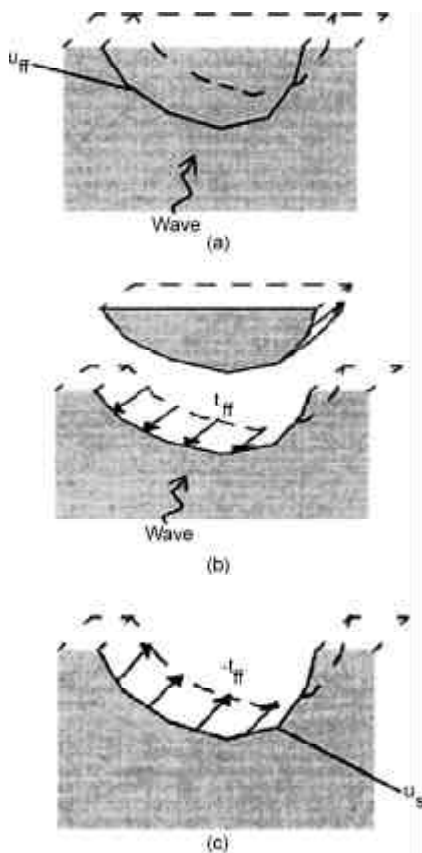
$$HU = GP \tag{5}$$

in which H is a $3n \times 3n$ matrix, U is a $3n \times 1$ displacement vector, G is a $3n \times 3nne$ matrix, and P is a $3nne \times 1$ traction vector, and nne is the product of the number of elements and number of nodes. The problem has $3n$ unknowns that should be obtained by solving Eq. (5).

4. Fundamental Solutions

The fundamental solution in the frequency domain for the displacement is the solution to Eq. (1) for a harmonic point force with unit amplitude applied at the point y in the l direction, i.e.,

$$\rho b = \delta(r)e^l \tag{6}$$

where r is the distance between the *observation point* x and the *source point* y, e^l the unit vector on l-direction and δ is the Delta Dirac function. In order to find the fundamental displacement solution, the principle of Helmholtz decomposition is used. The fundamental solution expressions are adopted from [31-32] and the free-field surface displacement in the frequency domain is:

$$u_{lk}^* = \frac{1}{\alpha \pi \rho c_2^2} \left[\psi \delta_{lk} - \chi r_{,l} r_{,k} \right] \tag{7a}$$

$$\psi = \frac{exp(-k_2 r)}{r} + \left(\frac{1}{k_2^2 r^2} + \frac{1}{k_2 r} \right) \frac{exp(-k_2 r)}{r}$$
$$- \frac{c_2^2}{c_1^2} \left(\frac{1}{k_1^2 r^2} + \frac{1}{k_1 r} \right) \frac{exp(-k_1 r)}{r} \tag{7b}$$

$$\chi = \left(\frac{3}{k_2^2 r^2} + \frac{3}{k_2 r} + 1 \right) \frac{exp(-k_2 r)}{r}$$
$$- \frac{c_2^2}{c_1^2} \left(\frac{3}{k_1^2 r^2} + \frac{3}{k_1 r} + 1 \right) \frac{exp(-k_1 r)}{r} \tag{7c}$$

in which u_{lk} denotes the displacement in a k direction when the load is applied in the l direction, $\alpha = 4$, δ_{ij} is Delta Dirac function and, $k_1 = \frac{i\omega}{c_1}$ and $k_2 = \frac{i\omega}{c_2}$ denote the wave numbers for compression and shear waves, respectively. The subscript l is used to indicate the coordinate direction of the point load.

The fundamental solution for the free-field surface tractions in the frequency domain is:

$$p_{lk}^* = \frac{1}{\alpha \pi} [(\frac{d\psi}{dr} - \frac{1}{r} \chi) (\delta_{lk} \frac{\partial r}{\partial n} + r_{,k} n_l)$$
$$- \frac{2}{r} \chi (n_k r_{,l} - 2 r_{,l} r_{,k} \frac{\partial r}{\partial n}) - 2 \frac{d\chi}{dr} r_{,l} r_{,k} \frac{\partial r}{\partial n} +$$
$$(\frac{c_1^2}{c_2^2} - 2)(\frac{d\psi}{dr} - \frac{d\chi}{dr} - \frac{\alpha}{2r} \chi) r_{,l} n_k] \tag{8a}$$

$$\frac{d\psi}{dr} = (-\frac{2}{r} - k_2 - \frac{3}{k_2 r^2} - \frac{3}{k_2^2 r^3}) \frac{exp(-k_2 r)}{r} +$$
$$\frac{c_2^2}{c_1^2} (\frac{1}{r} + \frac{3}{k_1 r^2} + \frac{3}{k_1^2 r^3}) \frac{exp(-k_1 r)}{r} \tag{8b}$$

$$\frac{d\chi}{dr} = (-\frac{4}{r} - k_2 - \frac{9}{k_2 r^2} - \frac{9}{k_2^2 r^3}) \frac{exp(-k_2 r)}{r}$$
$$+ \frac{c_2^2}{c_1^2} (\frac{4}{r} + k_1 + \frac{9}{k_1 r^2} + \frac{9}{k_1^2 r^3}) \frac{exp(-k_1 r)}{r} \tag{8c}$$

5. Treatment of Singularities

The solution for the free-field displacement and subsequently the matrix G contain singularities because of the $1/r$ term. A weak singularity is encountered when the collocation node coincides with the integration node. To perform the numerical integration using standard Gauss-Legendre quadrature over an element where the collocation node is one of the element nodes, a method proposed by Lachat is used [31]. In this method, the element is divided into a number of triangles, each having one of the corners at the collocation node and the integration is performed over each of the triangles using a standard Gauss-Legendre quadrature rule over an equivalent collapsed quadratic element, see Figure (3).
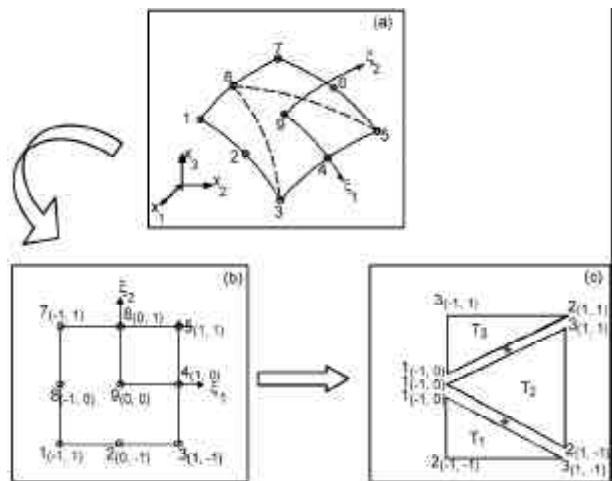

Figure 3. Division of 9-node quadrilateral element to proper triangular sub-elements with singularity at node 8.

In the collapsed quadrilateral elements, two of the corner nodes coincide, so that one of the element sides has a zero length. When performing the numerical integration over an element with such geometry, the Jacobian tends to zero as $r \to 0$ and cancels out the $1/r$ singularity. Subsequently the accuracy of the Gauss-Legendre quadrature is satisfactory.

The singularities of the free-field traction solution, and thus of the matrix H, are of the $1/r^2$ kind when the observation point coincides with the integration point. In this work, a numerical method is used to evaluate singular integrals for rigid body motion. This method normally applies only to closed domains. Ahmad and Banerjee [30] generalized the method for the 2-D case by using the enclosing elements technique to cover open domain boundaries where parts of the boundary are not discretized. Their method is employed to the 3-D case in this research.

The basis of the numerical method proposed by Dominguez [31] and others [32] for closed domains is that the singularity in the dynamic frequency domain solution arises from the static solution. By writing the total dynamic free-field solution matrix H for the traction as the summation of the static part, H_s, and the dynamic residue matrix, H_R, i.e.,

$$H = H_S + H_R \qquad (9)$$

special treatment is needed only for the singularities of the static part H_S. The remainder H_R can be determined using standard Gauss-Legendre quadrature, since it contains no singularities. For the 3-D case, the remainder term is derived by writing the exponential terms of the full elastodynamic solution as series expansions and subtracting the terms corresponding to the elastostatic fundamental solution [31]. Although the singular terms may be calculated analytically, this becomes complicated for complex geometries and therefore a numerical method for dealing with the singularities is preferred. The diagonal block of matrix H contains the tensor c_{ij} as well as the Cauchy principal value of the traction kernel integral [30], i.e.,

$$\overline{D}_{ij} = c_{ij} + \int_{S_1} \overline{F}_{ij} N_1 dS \qquad (10)$$

in which N_1 is the shape function for the singular node and S_1 is the area of the singular element. The corresponding equation for the static problem is:

$$D_{ij}^s = c_{ij} + \int_{S_1} F_{ij}^s N_1 dS \qquad (11)$$

From Eqs. (10) and (11) we can write:

$$\overline{D}_{ij} = D_{ij}^s + \int_{S_1} (\overline{F}_{ij} - F_{ij}^s) N_1 dS \qquad (12)$$

In Eq. (12), the diagonal blocks D_{ij}^s, which are the coefficients of the traction matrix for the static problem having the same geometry, can be obtained by using the rigid body motion, i.e.,

$$D_{ij}^s = c_{ij} + \int_{S_1} F_{ij}^s N_1 dS =$$

$$-[\sum_{\alpha=2}^{A} \int_{s_1} F_{ij}^s N_\alpha dS + \sum_{q=2}^{Q} \sum_{\alpha=1}^{A} \int_{s_q} F_{ij}^s N_\alpha dS] \qquad (13)$$

in which, A is the number of nodes in an element, and Q is the total number of elements. The method described above is obviously meaningless for an open domain as parts of the boundary are not included in the formulation. To overcome this problem, Ahmad and Banerjee [30] proposed that an artificial enclosing boundary be constructed merely for the evaluation of the singular diagonal terms of H_S and the constants related to the geometry. The basic assumption in this technique is that the displacements and tractions along the enclosing boundary at a sufficiently distant location have a negligible effect on the displacements along the modeled boundary. Using this scheme, the diagonal blocks D_{ij}^s of the H matrix are obtained by the summation of non-singular integrations of the static traction kernel over all the elements of the modeled boundary as well as enclosing elements, i.e.,

$$D_{ij}^s = -[\sum_{\alpha=2}^{A} \int_{s_1} F_{ij}^s N_\alpha dS + \sum_{q=2}^{Q} \sum_{\alpha=1}^{A} \int_{s_q} F_{ij}^s N_\alpha dS$$

$$+ \sum_{e=1}^{L} \sum_{\alpha=1}^{A} \int_{s_e} F_{ij}^s N_\alpha dS] \qquad (14)$$

where the third summation in Eq. (14) corresponds to the L enclosing elements. Once D_{ij}^s is evaluated, the diagonal blocks $\overline{D}_{ij}$ related to the dynamic problem can be easily found by using Eq. (12). Any closed region which has the correct local geometry for the true surface may be used instead of the original open region for the purpose of determining H. Any domain shape can be used for evaluating the diagonal terms of H_S as long as the following requirements are met:

1. The distance between the original elements and the new enclosing elements should be at least one element length to ensure sufficient precision.

2. The original geometry should be modeled correctly at the nodes. There is no contribution from the enclosing elements in the system of equations and also no extra degrees-of-freedom are introduced, because the enclosing elements are used only for integrating the static traction fundamental solution on the elements for which the *H* terms are to be found.

6. Numerical Results and Discussion

A special-purpose 3-*D* computer program was developed to implement the boundary element procedures for an incident plane wave with circular frequency ω. The propagation direction of the wave was defined by angles θ_h and θ_v corresponding to the angle of the ray (normal to wave front) from the horizontal *x*- and vertical *z*-axes, see Figure (1). The program can be used for canyons of arbitrary shape. The numerical examples of this section are designed to demonstrate the accuracy and efficiency of the method for different cases.

7. Validation Study

In order to obtain accurate results, the discretization should be fine enough and the 3D boundary element model should be large. The authors' studies lead to the fact that in order to obtain accurate results, the element size should be smaller than one-fourth of the shear wavelength. To establish the numerical accuracy of the method, problems involving the scattering of a harmonic plane *SH*-wave, for which results are available from previous works, are solved using the proposed method. In all cases, a semi-circular cross section of radius *R* cut in a homogenous half space is considered. The semi-cylindrical canyon and a length 1.5*R* of the free field on each side of the canyon are discretized as shown in Figure (4). The model has 180 nine-node
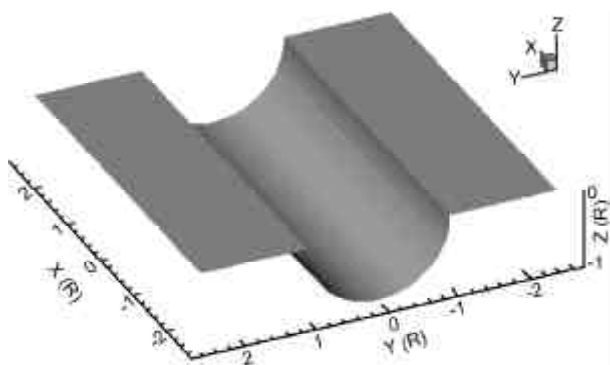
boundary elements with 777 nodes along the main boundary. A length 1.5*R* of the free field on each side of the canyon and a length 5*R* along the canyon axis are modeled. The results obtained by the boundary element (*BE*) method for a 2-D *SH* wave of unit amplitude impinging normal to the canyon axis is compared first with the exact solution by Trifunac [3]. The results presented in Figure (5) show the displacement amplitudes around the canyon for the horizontal angle of $\theta_h = 45°$ the vertical angles of $\theta_v = 1°$ and $45°$ for unit dimensionless frequency ($W = \omega R / \pi c_2 = 1$). A similar comparison is presented in Figure (6) for $\theta_v = \theta_h = 0$, which corresponds to a vertically incident *SH* wave with particle motion perpendicular to the axis of the canyon. For this test case the numerical result
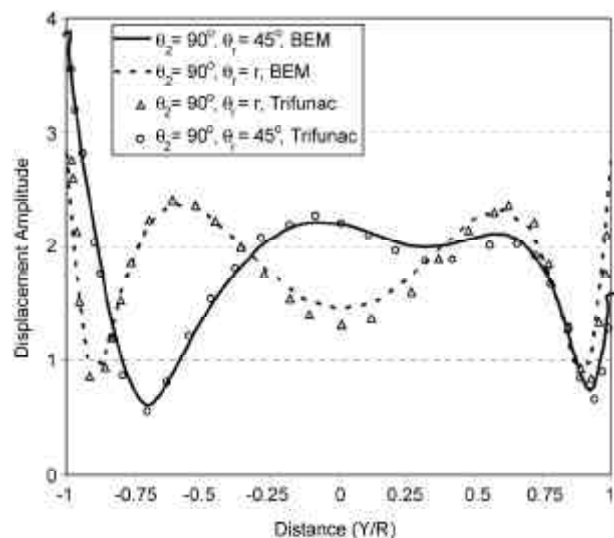

Figure 5. Displacement amplitudes obtained by the BE Method and by Trifunac for incident SH-Wave with Ω = 1.
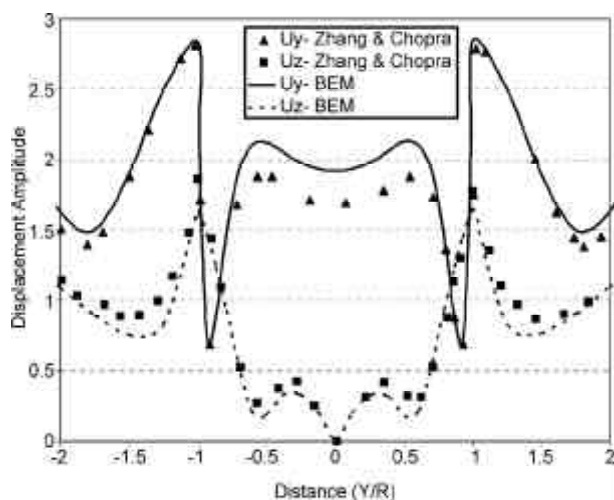

Figure 6. Displacement amplitudes versus relative distance obtained by the BE method and by Zhang and Chopra for incident SH-Wave with $\theta_h = 0$, $\theta_v = 0$ and Ω = 1.

Figure 4. Schematic picture of the semi-cylindrical canyon.

obtained by Zhang and Chopra [8] is used for the comparison. There is good agreement between results obtained by the *BE* method and the previous results. The finite length of the canyon and free-field has only a small effect on the computed displacements.

In order to investigate the effect of the free-field (both sides of the canyon cross-section) length (*Lh*) in finite 3*D* model on the accuracy of the results, two different free-field lengths (*Lh* = 1.5*R* and 3*R*) with the same canyon length (*L* = 5*R*) are considered and compared with each other in Figure (7). The results show that this parameter has a little effect on the accuracy of the results. Also in order to investigate the effect of the (model longitudinal) canyon length (*L*) on the accuracy of the results, different models with the same free-field length are analyzed. The results of these analyses are presented in Figure (8). These results show that the canyon length is more effective parameter than the free-field length in order to obtain accurate results. The long canyon gives more accurate results than the short one. Analysis with different lengths of canyon show that to obtain the results with an acceptable accuracy, (i.e., errors of less than 10%) one does not need to model beyond 10*R* length of the canyon. The same analysis with different lengths of the free-field is done and shows that in order to obtain sufficiently accurate results the free-field, surface should be discretized on both sides of the canyon over a distance of at least three times of the canyon radius.

8. Effects of Wave Characteristics

The results obtained for analysis with different dimensionless frequencies are shown in Figure (9). The results show that the variation of displacements across the canyon is more complicated for high dimensionless frequency than for low dimensionless frequency. At unit dimensionless frequency, the wavelength of the incident field is equal to the diameter of the valley; on the other hand for dimensionless frequency equal to 0.5, the wavelength of the incident field is equal to two times of the diameter of the valley. Hence for the dimensionless frequency equal to 0.5, the input wave does not detect the presence of the canyon as the scattering as well as for the unit dimensionless frequency case. As the wavelength of the input wave becomes comparable to the characteristic length of the canyon, more complicated wave pattern of the scattered field is expected.
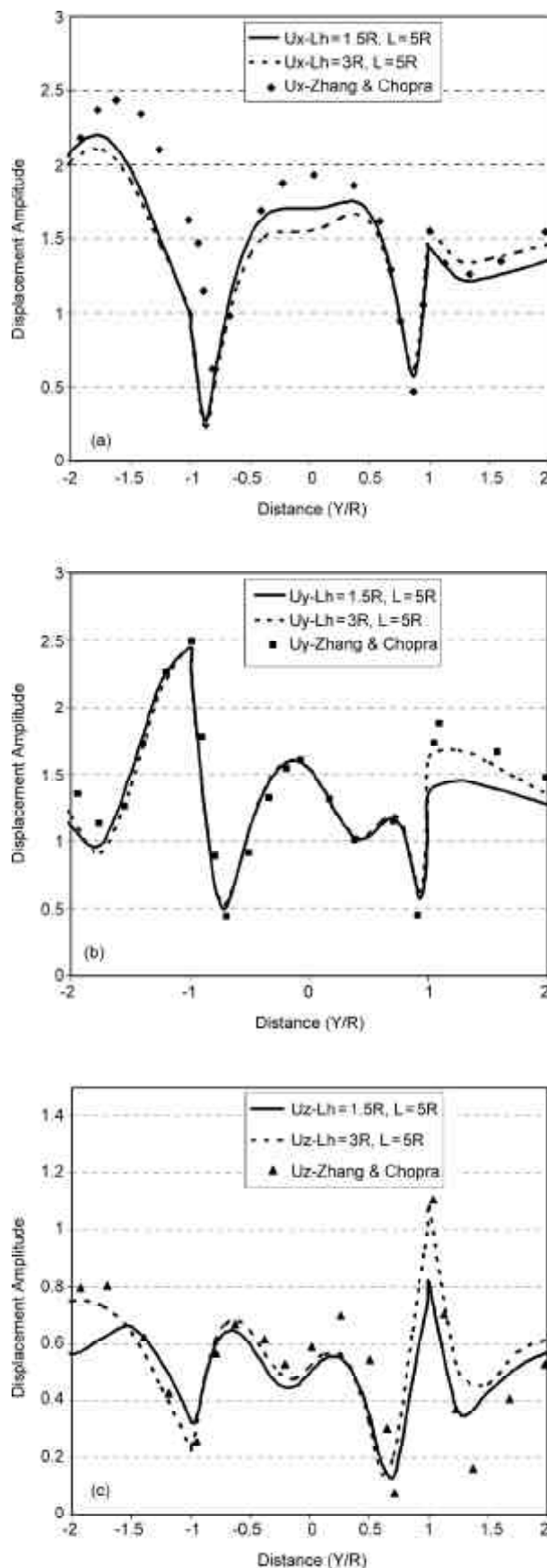

Figure 7. Displacement amplitude versus relative distance for two different free-field lengths calculated by the BE method and by Zhang and Chopra for incident SH-Wave with $\theta_h = 45, \theta_v = 45$ and $\Omega = 1$.
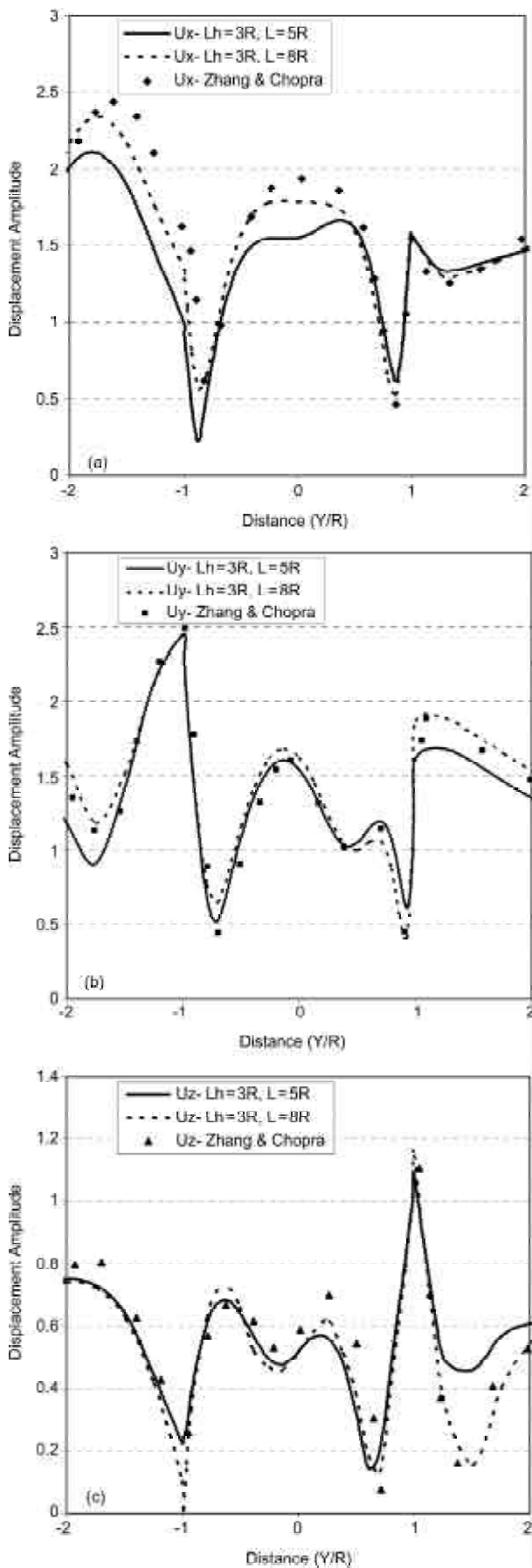
Figure 8. Displacement amplitude versus relative distance for two different canyon lengths calculated by the BE method and by Zhang and Chopra for incident SH-Wave with $\theta_h = 45$, $\theta_v = 45$ and $\Omega = 1$.
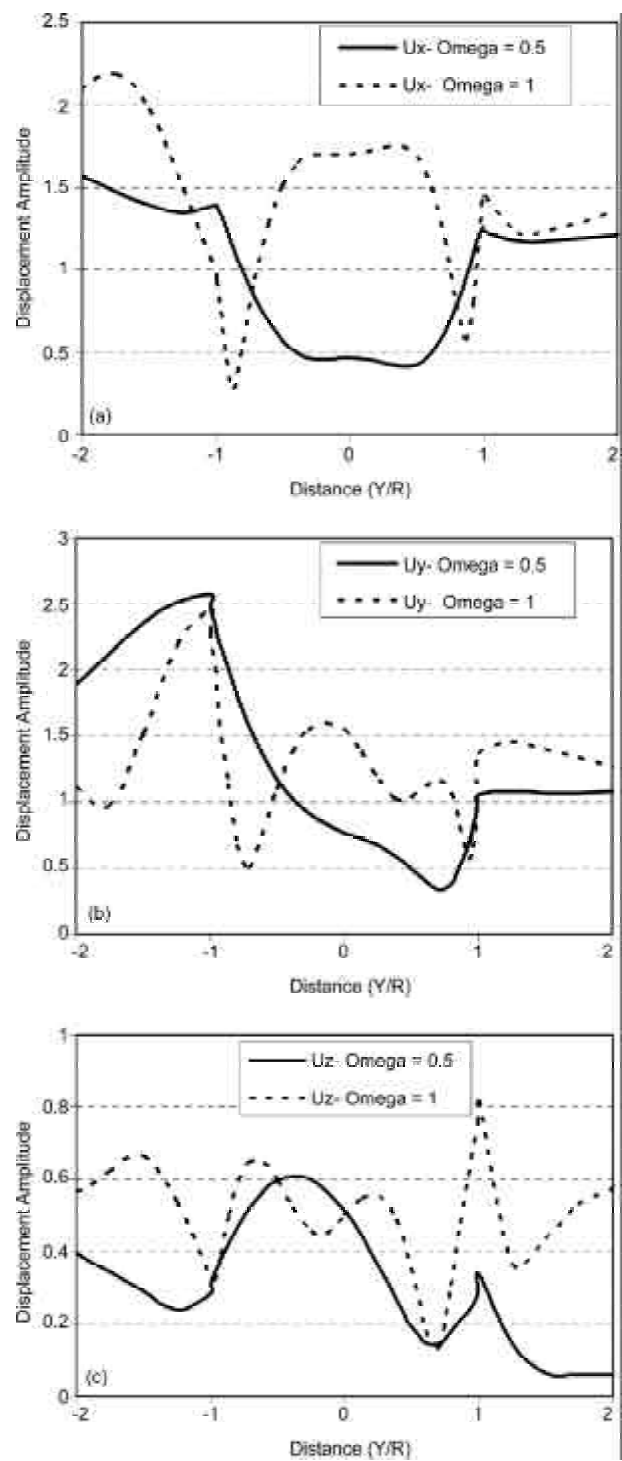

Figure 9. Comparison of results obtained for two different dimensionless frequency ($\Omega = 0.5$ and $\Omega = 1$) for incident SH-Wave with $\theta_h = 45$ and $\theta_v = 45$.

Analyses for different wave incident angles with unit dimensionless frequency have been completed and results are presented in Figure (10). Different patterns of the displacement variation across the canyon are achieved for different wave incident angles. It is shown that wave incident angle is one of the most important parameter on the pattern of the displacement variation across the canyon.
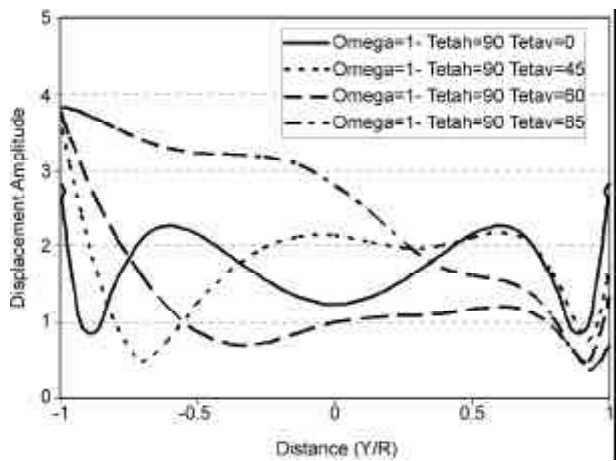
Figure 10. The results obtained for different wave incident angles with unit dimensionless frequency for incident SH-Wave.

9. Effects of Material Parameters

The effect of material properties of half space such as damping ratio and poisson's ratio are investigated by different analysis and are illustrated in Figures (11) and (12), respectively. The results show that these parameters do not affect the pattern of the displacement variation across the canyon but in order to get accurate results of topographic phenomenon, these parameters should be evaluated precisely. The system with damping may induce large displacements in the side of the canyon located in the wave arriving direction in comparison to system without damping. In general, the difference of maximum displacements obtained in both sides of the canyon is increasing with damping.

10. Effects of Canyon Geometry

In order to investigate the effect of the canyon geometry on the topographic amplification, the model of a semi-elliptical canyon as illustrated in Figure (13) is considered and analyzed. The results are compared with results of the canyon with the semi-circular cross section canyon. The large diameter of semi-elliptical canyon is considered to be $2R$ (in the y-direction) and the small diameter is R (in the z-direction). This model can also be used to investigate the effect of the depth of the canyon due to this fact that the only difference between two models is the depth of points located on the canyon. The results obtained for two different dimensionless frequencies for these models are presented in Figures (14) and (15). It can be concluded that the effect of canyon shape and canyon depth on the
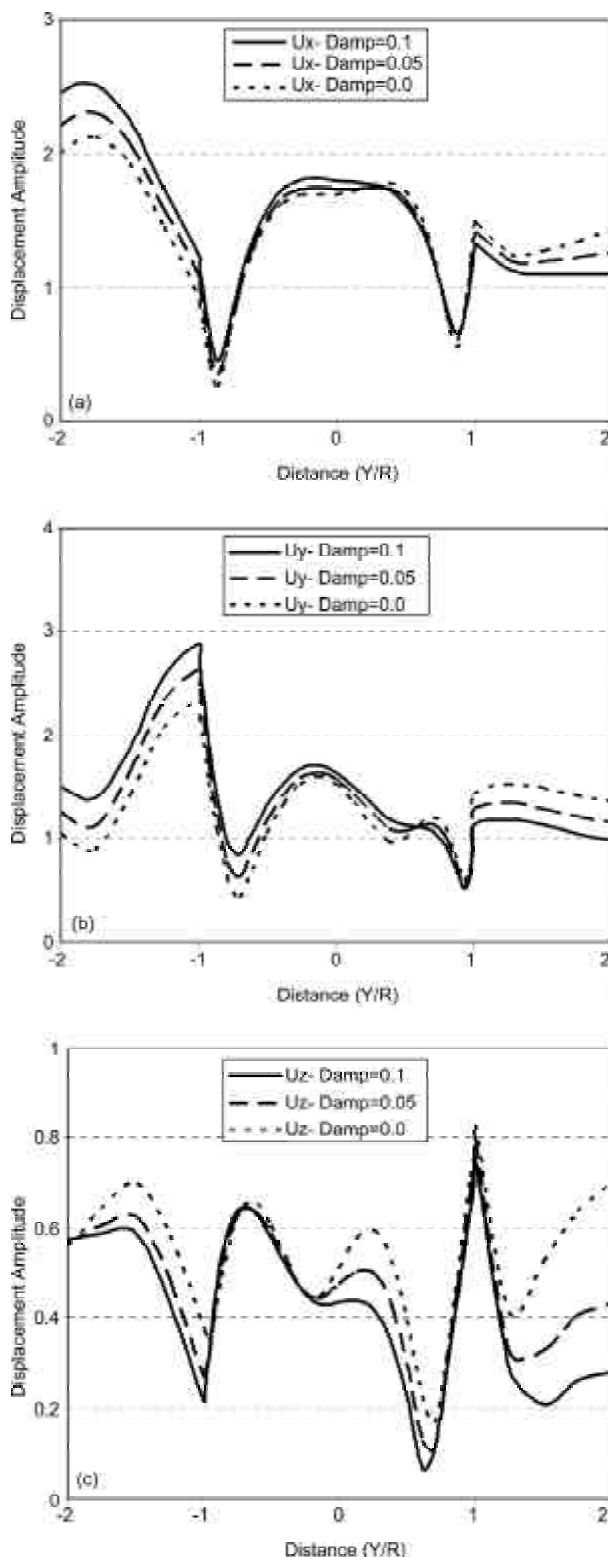

Figure 11. Comparison of results obtained for different damping ratio for incident SH-Wave with $\theta_h = 45$, $\theta_v = 45$ and $\Omega = 1$.

topographic amplification is frequency dependent. On the other hand, comparison for same frequencies shows that the topographic effect depends on the canyon shape and depth, too. Results obtained for two different dimensionless frequency show that the

deep canyon (semi-circular canyon) has more amplification effect on displacement amplitude along the canyon in comparison to shallow canyon (semi-elliptical canyon). For small dimensionless frequency, the wavelength of the incident wave is larger than the characteristic length of the canyon as depth for semi-elliptical one rather than semi-circular one. In this case the existence of the semi-elliptical valley is less detected and therefore the scattered wave field is not complicated. Results obtained for high dimensionless frequency is more sensitive to increasing of the depth of the canyon than for low dimensionless frequency.
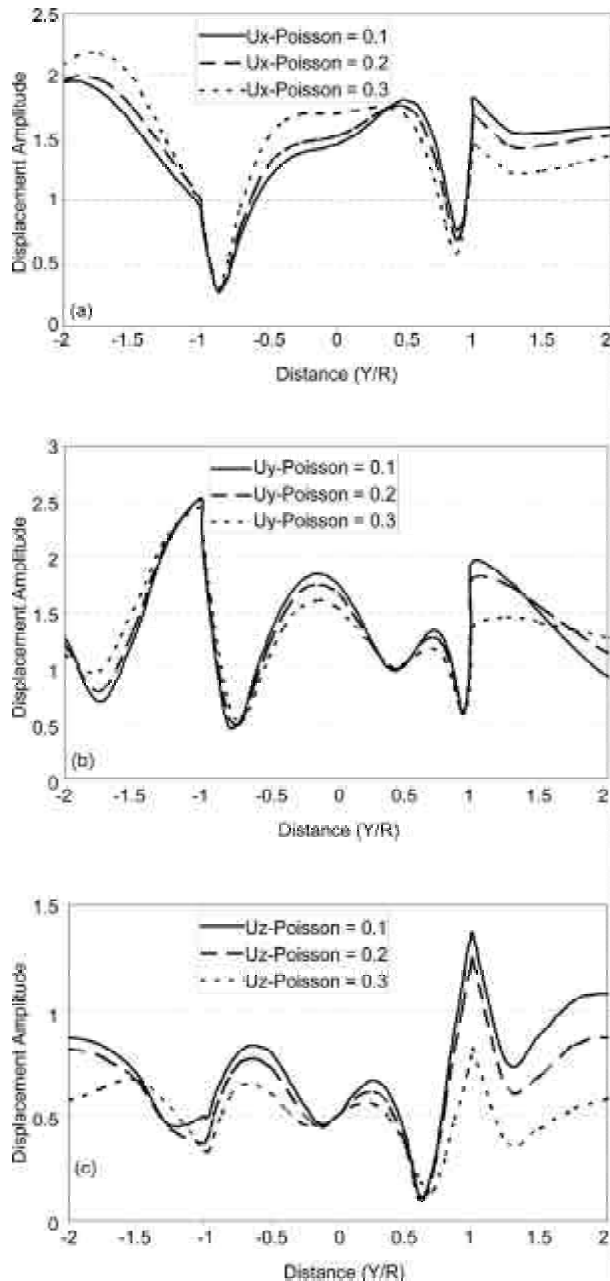

Figure 12. Comparison of results obtained for different Poisson's ratio for incident SH-Wave with $\theta_h = 45$, $\theta_v = 45$ and $\Omega = 1$.
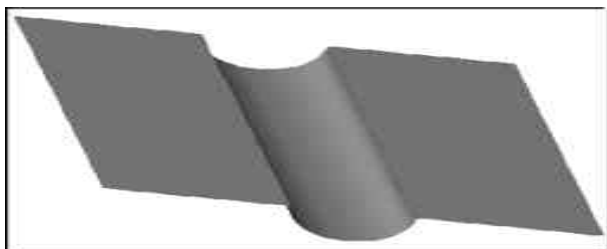

Figure 13. A schematic picture of the semi-elliptical canyon.
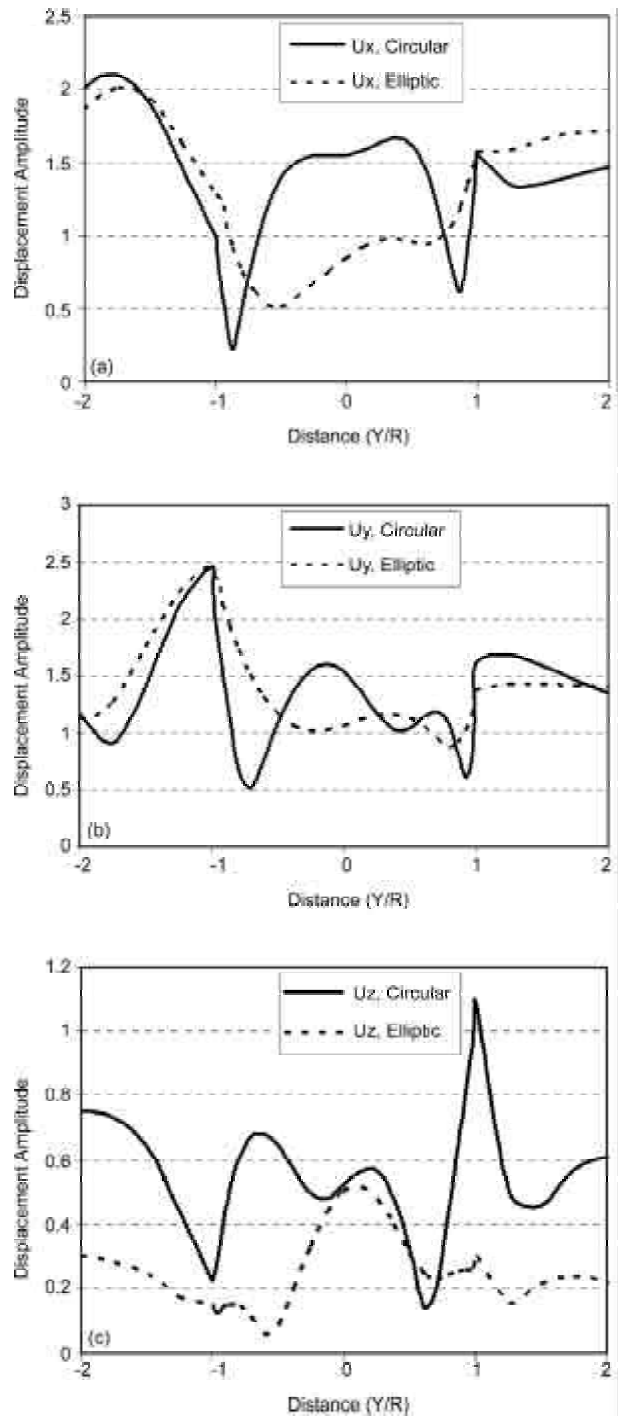

Figure 14. Comparison of results obtained for canyons with different shapes for incident SH-Wave with $\theta_h = 45$, $\theta_v = 45$ and $\Omega = 1$.
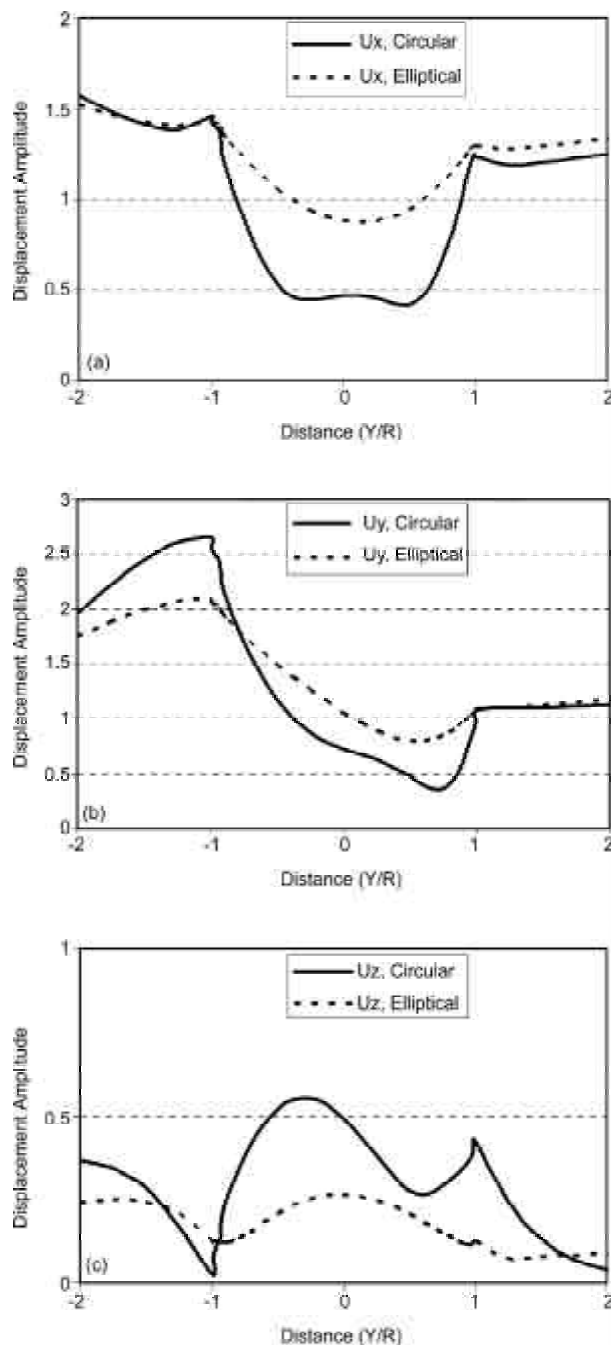
Figure 15. Comparison of results obtained for canyons with different shapes for incident SH-Wave with $\theta_h = 45$, $\theta_v = 45$ and $\Omega = 1$.

11. Conclusions

The multi-domain boundary element method proposed by Ahmad and Banerjee [30] is employed to three dimensional wave propagation problems. Results from this method are compared to previous results obtained by Trifunac [3] and Zhang and Chopra [8]. This method yields sufficiently accurate results and can be used for real-world problems with complex topographies.

Effects of different parameters are investigated and the following results obtained:

The free-field (both sides of the canyon cross-section) length is less influential on the accuracy of results than the (model longitudinal) canyon length. Analysis with different lengths of canyon and free-field show that in order to obtain sufficiently accurate results, one does not need to go beyond $10R$ and $3R$ (R, being the canyon section effective radius), respectively.

It is shown that the material properties as well as the wave incident angle and frequency have considerable effects on the wave scattering problems. When applying usual values of damping, the damped system may induce larger displacements on the side of the canyon located on the wave incident direction in comparison to system without damping. Wave parameters (direction and frequency) affect the pattern of the displacement variation across the canyon. On the other hand, material properties (damping value and poisson's ratio) have only negligible effects on the pattern of the displacement variation.

The effect of canyon shape and canyon depth on the topographic amplification is frequency dependent. The amplification of displacement has a direct relationship with the canyon depth. Deep canyons induce more amplification effects than shallow canyons in different dimensionless frequencies.

For high dimensionless frequencies, the obtained results are more sensitive to the canyon depth than for low dimensionless frequencies.

References

1. Celebi, M. (1987). "Topographical and Geological Amplifications Determined from Strong-Motion and Aftershocks Records of the 3 March 1985 Chile Earthquake", Bulletin of the Seismological Society of America, **77**, 1147-1167.

2. Eurocode 8 (1996). "Design Provisions for Earthquake Resistance of Structures, Part 5. Foundations, Retaining Structures and Geotechnical Aspects".

3. Trifunac, M.D. (1973). "Scattering of Plane SH-Waves by a Semi-Cylindrical Canyon", *Earthquake Engineering and Structural Dynamics*, **1**, 267-281.

4. Pedersen, H.A., Sanchez-Sesma, F.J., and Campillo, M. (1994). "Three-Dimensional Scattering by Two-Dimensional Topographies", Bulletin of the Seismological Society of America,

84(4), 1169-1183.

5. Sanchez-Sesma, F.J. and Luzon, F. (1995). "Seismic Response of Three-Dimensional Aluuvial Valleys for Incident P, S, and Rayleigh Waves", Bulletin of the Seismological Society of America, **85**(1), 269-284.

6. Sanchez-Sesma, F.J. and Campillo, M. (1993). "Topographic Effects for Incident P, SV, and Rayleigh Waves", *Tectonophysics*, **218**,113-125.

7. Paolucci, R. (2002). "Amplification of Earthquake Ground Motion by Steep Topographic Irregularities", *Earthquake Engineering and Structural Dynamics*, **31**, 985-998.

8. Zhang, L. and Chopra, A.K. (1991). "Three-Dimensional Analysis of Spatially Varying Ground Motions Around a Uniform Canyon in a Homogeneous Half-Space", *Earthquake Engineering and Structural Dynamics*, **20**, 911-926.

9. Niu, Y. and Dravinski, M. (2003). "Direct 3D BEM for Scattering of Elastic Waves in a Homogeneous Anisotropic Half-Space", *Wave Motion*, **38**(2), 165-175.

10. Dravinski, M. (2003). "Scattering of Elastic Waves by a General Anisotropic Basin. Part 2: a 3D model", *Earthquake Engineering and Structural Dynamics*, **32**(5), 653-670.

11. Eshraghi, H. and Dravinski, M. (1989). "Scattering of Plane Harmonic SH, SV, P and Rayleigh Waves by Non-Axisymmetric Three Dimensional Canyons: A Wave Function Expansion Approach", *Earthquake Engineering and Structural Dynamics*, **18**(7), 983-998.

12. Mossessian, T.K. and Dravinski, M. (1990). "Amplification of Elastic Waves by a Three Dimensional Valley. Part1: Steady-State Response", *Earthquake Engineering and Structural Dynamics*, **19**, 667-680.

13. Zhao, C., Valliappan, S., and Wang, Y.C. (1992). "A Umerical Model for Wave Scattering Problems in Infinite Media Due to P- and SV-Wave Incidences", *International Journal for Numerical Methods in Engineering*, **33**(8), 1661-1682.

14. Luco, J.E., Wong, H.L., and De Barros, F.C.P. (1990). "Three Dimensional Response of a Cylindrical Canyon in a Layered Half-Space", *Earthquake Engineering and Structural Dynamics,* **19**, 799-817.

15. Athanasopoulos, G.A., Pelekis, P.C., and Leonidou, E.A. (1999). "Effects of Surface Topography on Seismic Ground Response in the Egion (Greece) 15 June 1995 Earthquake", *Soil Dynamics and Earthquake Engineering*, **18**, 135-149.

16. Assimaki, D., Kausel, E., and Gazetas, G. (2004). "Topography Effects in the 1999 Athens Earthquake: Engineering Issues in Seismology", *Proceedings 11th ICSDEE and 3rd ICEGE*, UC Berkeley, **2**, 31-38.

17. Kamalian, M., Jafari, M.K., Sohrabi, A., Razmkhah, A., and Gatmiri, B. (2006). "Time-Domain Two-Dimensional Response Analysis of Non-Homogeneous Topographic Structures by a Hybrid BE/FE Method", *Soil Dynamics and Earthquake Engineering*, **26**, 753-765.

18. Kamalian, M., Jafari, M.K., and Sohrabi, A. (2003). "On Time-Domain Two-Dimensional Site Response Analysis of Topographic Structures by BEM", *Journal of Seismological Earthquake Engineering*, **5**(2), 35-45.

19. Geli, L., Bard, P.Y., and Jullien, B. (1988). "The Effect of Topography on Earthquake Ground Motion: A Review and New Results", Bulletin of Seismological Society of America , **78**(1), 42-63.

20. Vahdani, S. and Wikstorm, S. (2002). "Response of Tarzana Strong Ground Motion Site During the 1994 Northridge Earthquake", *Soil Dynamics and Earthquake Engineering*, **22**, 837-848.

21. Zaslavsky,Y., Shapira, A., and Arzi, A.A. (2000). "Amplification Effects from Earthquakes and Ambient Noise in the Dead Sea Rift (Israel)", *Soil Dynamics and Earthquake Engineering*, **20**, 187-207.

22. Levert, L.C. (1986). "The Province Earthquake of June 11th, 1999 (France) New Assessment of Near-Field Effects", *Proc. of the VIII European Conference on Earthquake Engineering*, Lisbon, **2**, 42-79.

23. Brambati A., Faccioli, E., Carulli, E., Culchi, F., Onofri, R., Stefanini, S., and Ulcigrai, F. (1980). "Studio di Microzonazione Sismica Dell'area Di Tarcento (Friuli) Regione Autonoma Friuli-Veneia-Giuli (ed)", (in Italian).

24. Sirovich, L. (1982). "Southern Italy November 23, 1980 Earthquake", *Proc. of the Seventh European Conference of Earthquake Engineering*, Athens, Greece, **7**, 419-429.

25. Pederesen, H., Le Brun, B., Hatzfeld, D., Campillo, M., and Bard, P-Y.(1994). "Ground-Motion Amplitude Across Ridges", Bulletin of Seismological Society of America, **84**,1786-1800.

26. Chavez-Garcia, F.J., Sanchez, L.R., and Hatzfeld, D. (1996). "Topographic Site Effects and HVSR. A Comparison Between Observations and Theory", Bulletin of Seismological Society of America, **86**, 1559-1573.

27. Chavez-Garcia, F.J., Rodriguez, M., Field, E.H., Hatzfeld, D. (1997). "Topographic Site Effects. A Comparison of the Two Nonreference Methods", *Bulletin of Seismological Society of America*, **87**, 1667-1673.

28. Paolucci, R., Faccoli, E., and Maggio, F. (1999). "3D Response Analysis of An Instrumented Hill at Matsuzaki, Japan, by a Spectral Method", *J. Seismology*, **3**, 191-209.

29. Bouchon, M. and Sanchez-Sesma, F.J. (2007). "Boundary Integral Equations and Boundary Elements Methods in Elastodynamics", *Advances in Geophysics*, **48**, 157-189.

30. Ahmad, S. and Banerjee, P.K. (1988). "Multi-Domain BEM for Two Dimensional Problems of Elastodynamics", *Int. Journal for Numerical Methods in Engineering*, **26**, 891-911.

31. Dominguez, J. (1993). "Boundary Elements in Dynamics", Elsevier.

32. Manolis, G.D. and Beskos, D.E. (1988). "Boundary Element Methods in Elastodynamics", Elsevier.